Dynamic Modeling and Anti-swing Control of Double Pendulum Payload System of Overhead Crane

Zizheng Liu[1], Shenghai Wang[2], Haiquan Chen[2], Guoyuan Li[1], Houxiang Zhang[1]

Abstract— **In this paper, an anti-swing controller for a double pendulum payload system is proposed using the method of backstepping based on dynamic models. Lagrange equations are used to derive the dynamic equations of the overhead crane payload system in a 2-dimensional plane, which provides an elegant clean form for developing the controller. The anti-swing control system, as well as the simulations, is implemented in real-time via the software tool MATLAB/Simulink. The results prove that the proposed controller can effectively help the system eliminate the induced swing of the payload system in a short period.**

I. Introduction

Cranes are widely used as important equipment to handle and transfer objects in various occasions and fields such as factories, harbors, and offshore. Crane operation is vital to the performance of cranes, which has attracted increasing attention from various fields. Today, the development of technology and industrialization has accelerated the evolution of cranes in the direction of more automation, digitalization, and intelligence [1].

To maximize efficiency, the crane is required to move as fast as possible in most cases. However, during its starting and stopping, the swing of the payload will be induced inevitably due to all kinds of interferences such as friction, system vibration caused by payload inertia and cable flexibility [2]. This kind of swing can be approximately regarded as undamped vibration. The system can only rely solely on the resistance of the air to eliminate the swing of the payload if no other external force is applied, which has an adverse impact on the crane efficiency [3] and also increases the possibility of accidents, especially for vulnerable or dangerous surroundings [4].

The last decades have seen an increasing improvement in developing anti-swing control strategies for different kinds of cranes [5]. Due to the complicated dynamics and underactuated characteristics of the crane system [6], the control strategy is gradually developing towards the trend of intelligent control. Compared with traditional control methods, artificial intelligence-based control methods such as fuzzy control [7, 8], neural network control [9, 10] can better incorporate the human experience to improve control performance. Also, traditional control methods tend to be combined with intelligent control. For example, as a classic method to design closed-loop system controllers in the field of engineering, PID now is mostly applied combined with intelligent control methods such as fuzzy control [11, 12]. In parallel, some advanced control methods are considered as effective methods to solve anti-swing problems such as sliding mode control [13] and optimal control [14].

Generally speaking, the swing of the payload presents the characteristics of a single pendulum. However, in engineering practice, the payload system of the crane is going to show the characteristics of a double pendulum as the mass of the hook is not negligible compared with the mass of the payload [15].

An anti-swing controller is proposed in this paper, using the method of backstepping which is for designing stabilizing controls for a special class of dynamical systems. Backstepping has obvious advantages in designing robust or adaptive controllers for uncertain systems, especially when disturbances or uncertainties do not satisfy matching conditions. Now it has received extensive attention and has been extended to more fields, such as output regulation, adaptive control.

This paper develops an effective control approach for overhead crane operations that provides anti-swing combined functionalities. The rest of the paper is organized as follows. In Section II, the overhead crane and Lagrange equations are briefly introduced, which enables the derivation of the dynamic equations of the double pendulum payload system. In Section III, two influence factors are taken into consideration analyzing in different conditions. Section IV describes the process of the proposed controller in detail. In Section V, simulations are implemented in real-time to verify the effectiveness of the control system. The conclusion and future works are outlined in Section VI.

II. Dynamic Modeling

A. The Overhead Crane

An overhead crane, commonly referred to as a bridge crane, is a type of crane found in industrial environments, which allows you to lift and move heavy payloads from one location to another in a precise manner. There are various types of overhead cranes, but their structures are generally not significantly varied. One general overhead crane is shown in Fig. 1. It is normally comprised of two parallel tracks that sit on longitudinal I-beams and are bolted to opposing steel columns using brackets. The two parallel tracks are called the bridge, more often referred to as a single girder or double girder design. The payload is supported by a hook that connects to the hoist. A trolley supports the payload system and moves horizontally along the bridge to position before picking up or lowering a load.

The author would like to thank China Scholarship Council for funding his research at Norwegian University of Science and Technology.

[1]Zizheng Liu, Houxiang Zhang, Guoyuan Li are with the Department of Ocean Operations and Civil Engineering, Norwegian University of Science and Technology, 6009 Aalesund, Norway. ({zizheng.liu, hozh, guoyuan.li} @ntnu.no)

[2]Shenghai Wang, Haiquan Chen are with the Department of Marine Engineering, Dalian Maritime University, Dalian, China.

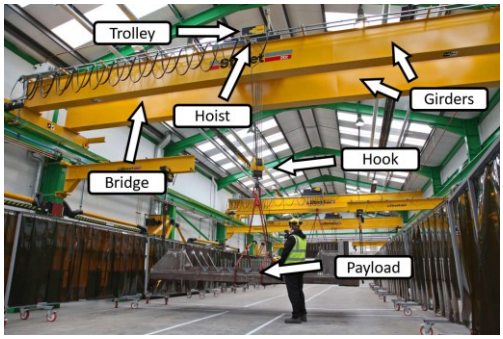

Figure 1. Overhead crane

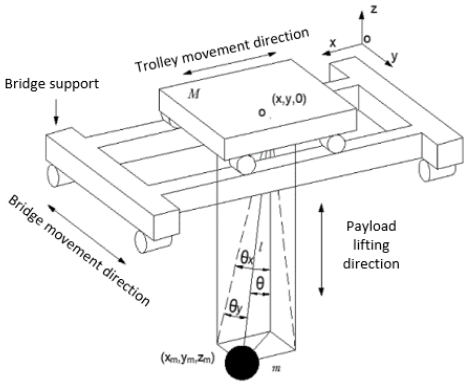

Figure 2. Simplified 3D model of overhead crane

B. Lagrange Equations

Various approaches enable the derivation of dynamical equations for mechanical systems. All of them result in equivalent sets of equations. However, they are presented in different forms suitable for different purposes of computation and interpretation. As one of the best-known methods to solve dynamic problems with constraints, Lagrange equations are the ones of motion of any complete system expressed in generalized coordinates, which are established from the viewpoint of energy with the kinetic energy, potential energy, and generalized forces of the system to be analyzed together. A general and comprehensive description of the Lagrange method for computing robot dynamics is given in [16].

The general form of the ideal complete Lagrange equation which is the so-call Lagrange equations of the first kind is:

$$\frac{d}{dt}\left(\frac{\partial T}{\partial \dot{q}_\alpha}\right)-\frac{\partial T}{\partial q_\alpha}=Q_\alpha \ ,\alpha=1,2,3...,\mathrm{s} \tag{1}$$

where T is the kinetic energy; Q is the generalized inertia force; q is the generalized coordinate; $\dot{q}$ is the generalized velocity; α is the number of system variables.

For the crane payload system, Lagrange equations of the second kind can be used to solve the problem. The equations do not include constraint forces at all, only non-constraint forces need to be accounted for, which is also called Euler–Lagrange equations:

$$\frac{d}{dt}\left(\frac{\partial L}{\partial \dot{q}_\alpha}\right)-\frac{\partial L}{\partial q_\alpha}=0 \tag{2}$$

And L is the Lagrangian expressed as:

$$L(q,\dot{q})=T(q,\dot{q})-V(q,\dot{q}) \tag{3}$$

where V is the potential energy of the system.

C. Dynamic Equations

During the operation of the overhead crane, the payload will present a kind of spherical movement, which takes the connection point between the trolley and the main cable as the center and takes the length of the cable as the radius, as shown in Fig. 2. This kind of pendulum happens in three-dimensional space, but it can be regarded as the result of the coupling of two kinds of pendulum in two-dimensional planes [17].

Considering that the crane will be subject to various disturbances in practical operation, the following assumptions must be assumed for modeling the dynamics in the simplification process.

(1) The bridge and the trolley work separately.

(2) The deformation of the crane support and girders, as well as the height difference of the track is negligible.

(3) The friction between the trolley and the track is negligible.

(4) All cables feature sufficient strength and stiffness, the mass of the cable is neglected, and changes in cable length due to force are negligible.

(5) The payload has a regular shape and can be regarded as a particle, and the torsional motion of the payload with the cable as the axis can be neglected.

(6) The damping from the air and the wind is negligible.

Table I lists the physical properties used during the modeling.

TABLE I. PHYSICAL PROPERTIES

Property	Symbol	Value	Unit
Hook mass	m_1	constant	kg
Payload mass	m_2	constant	kg
Trolley displacement	x	variable	m
Trolley velocity	$\dot{x}$	variable	m/s
Trolley acceleration	$\ddot{x}$	variable	m/s^2
Cable length	l	variable	m
Cable velocity	$\dot{l}$	variable	m/s
Cable acceleration	$\ddot{l}$	variable	m/s^2
Payload angle	θ	variable	deg
Payload angular velocity	$\dot{\theta}$	variable	deg/s
Payload angular acceleration	$\ddot{\theta}$	variable	deg/s^2
Gravity	g	9.80	m/s^2

According to the assumption, when the overhead crane carries a payload, the payload system presents the characteristics of a double pendulum. In this case, the hook

and the payload can be treated as a first-order pendulum and a second-order pendulum respectively, the model of which can be shown in Fig. 3.

It can be seen that the coordinate of the trolley position is $(0, x_t)$, and the coordinates of the first-order pendulum (x_1, y_1) and the second-order pendulum (x_2, y_2) are expressed as:

$$\begin{cases} x_1 = x_t + l_1 \sin\theta_1 \\ y_1 = -l_1 \cos\theta_1 \end{cases} \tag{4}$$

$$\begin{cases} x_2 = x_t + l_1 \sin\theta_1 + l_2 \sin\theta_2 \\ y_2 = -l_1 \cos\theta_1 - l_2 \cos\theta_2 \end{cases} \tag{5}$$

The total kinetic energy T of the crane payload system can be calculated as:

$$\begin{aligned} T &= \frac{1}{2} m_1 (\dot{x}_1^2 + \dot{y}_1^2) + \frac{1}{2} m_2 (\dot{x}_2^2 + \dot{y}_2^2) \\ &= \frac{1}{2} m_1 \left(\left(\dot{x}_t + l_1 \dot{\theta}_1 \cos\theta_1 \right)^2 + l_1^2 \dot{\theta}_1^2 \sin\theta_1^2 \right) \\ &\quad + \frac{1}{2} m_2 \left(\left(\dot{x}_t + l_1 \dot{\theta}_1 \cos\theta_1 + l_2 \dot{\theta}_2 \cos\theta_2 \right)^2 + \left(l_1 \dot{\theta}_1 \sin\theta_1 + l_2 \dot{\theta}_2 \sin\theta_2 \right)^2 \right) \end{aligned} \tag{6}$$

The horizontal plane of the trolley is assumed to be the zero potential energy plane of the system, then the total potential energy V of the system is:

$$V = -g l_1 m_1 \cos\theta_1 + g m_2 \left(-l_1 \cos\theta_1 - l_2 \cos\theta_2 \right) \tag{7}$$

Using Lagrange equations to solve the model of the entire system, the dynamic expression of the system can be obtained after linearization, where the Lagrange equation with the pendulum angle of the first-order pendulum as the generalized coordinate $q_\alpha = \theta_1$ is:

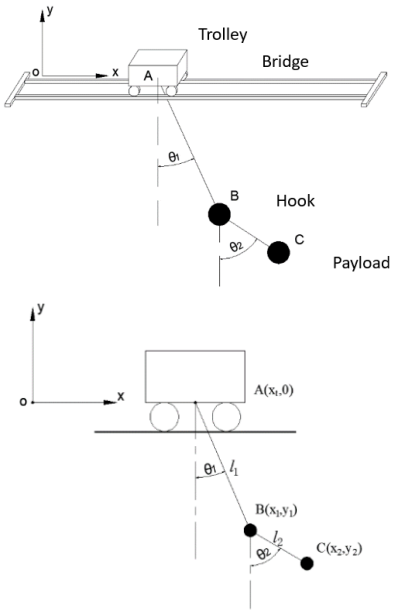

Figure 3. Simplified model of overhead crane double pendulum system

$$\begin{aligned} & l_1 \left(m_1 + m_2 \right) \left(\ddot{x}_t \cos\theta_1 + g \sin\theta_1 + l_1 \ddot{\theta}_1 \right) \\ & + l_1 l_2 m_2 \ddot{\theta}_2 \cos(\theta_1 - \theta_2) + l_1 l_2 m_2 \dot{\theta}_2^{\,2} \sin(\theta_1 - \theta_2) = 0 \end{aligned} \tag{8}$$

where Lagrange equation with the pendulum angle of the second-order pendulum as the generalized coordinate $q_\alpha = \theta_2$ is:

$$\begin{aligned} & l_2 m_2 \ddot{x}_t \cos\theta_2 + l_1 l_2 m_2 \ddot{\theta}_1 \cos(\theta_1 - \theta_2) + l_2^2 m_2 \ddot{\theta}_2 \\ & - l_1 l_2 m_2 \dot{\theta}_1^{\,2} \sin(\theta_1 - \theta_2) + l_2 m_2 g \sin\theta_2 = 0 \end{aligned} \tag{9}$$

III. Dynamic Analysis

Compared with the single pendulum system, the double pendulum system has an additional impact on the second-order pendulum. For this reason, the impact of the first-order pendulum amplitude and the length of the second-order pendulum cable on the swing of the double pendulum system are analyzed separately based on the single pendulum system. The following figures show the plotting of both orders' pendulum angles in different cases.

A. The Amplitude of the First-order Pendulum

Fig. 4 shows the swing angles of the double pendulum for different amplitudes of the first-order pendulum, where the cable lengths are set as 1 m and 0.25 m. It can be seen that the amplitude and frequency of the second-order pendulum are more severe than those of the first-order pendulum when the cable length of the double pendulum is a constant. The maximum value of the second-order pendulum is about 1.6-1.7 times the initial swing angle of the first-order pendulum.

B. The Cable Length of the Second-order Pendulum

Fig. 5 shows the swing angles of the double pendulum with different cable lengths of the second-order pendulum, where the cable length and the amplitude of the first-order pendulum are respectively set as 1m and 10 degrees.

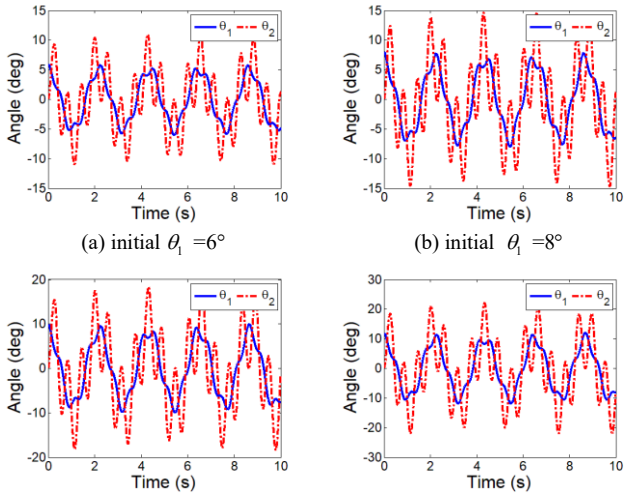

(a) initial θ_1 =6° (b) initial θ_1 =8°

(c) initial θ_1 =10° (d) initial θ_1 =12°

Figure 4. The impact of the amplitude of the first-order pendulum on the swing of the double pendulum

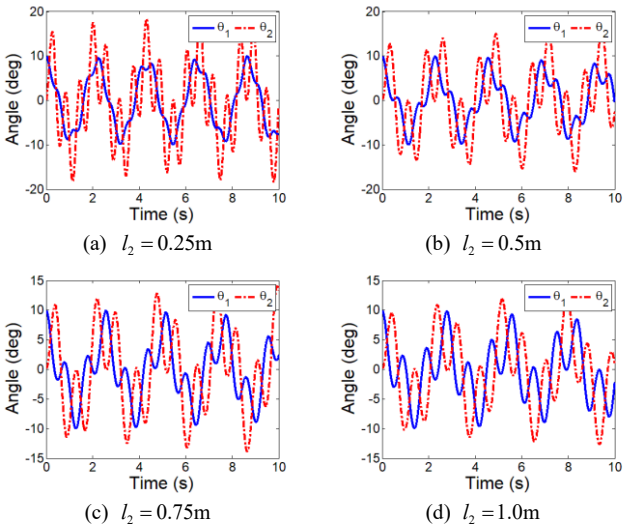

(a) $l_2 = 0.25$m (b) $l_2 = 0.5$m

(c) $l_2 = 0.75$m (d) $l_2 = 1.0$m

Figure 5. The impact of the cable length of the second-order pendulum on the swing of the double pendulum

It can be seen that when the cable length of the first-order pendulum is a constant, the swing amplitude of the second-order pendulum decreases as the cable length of the second-order pendulum increases, while the varying swing amplitude of the second-order pendulum changes the swing amplitude and frequency of the first-order pendulum.

IV. Controller Design

To eliminate the swing of the double pendulum of the crane payload system, an anti-swing controller was developed by applying the method of backstepping.

State variables of the system are chosen as:

$$\begin{aligned}\mathbf{X}_1 &= \begin{bmatrix} x & \theta_1 & \theta_2 \end{bmatrix}^{\mathrm{T}} \\ \mathbf{X}_2 &= \begin{bmatrix} \dot{x} & \dot{\theta}_1 & \dot{\theta}_2 \end{bmatrix}^{\mathrm{T}} \\ \mathbf{X}_3 &= \begin{bmatrix} \ddot{x} & \ddot{\theta}_1 & \ddot{\theta}_2 \end{bmatrix}^{\mathrm{T}}\end{aligned} \tag{10}$$

where $\mathbf{X}_3$ can be written in another form if the input is written like $u = x_t$:

$$\mathbf{X}_3 = \mathbf{f}(\mathbf{x}) + \mathbf{b}(\mathbf{x})u \tag{11}$$

where $\mathbf{f}(\mathbf{x}) = \begin{bmatrix} f_1(x) & f_2(x) & f_3(x) \end{bmatrix}^{\mathrm{T}}$ and $\mathbf{b}(\mathbf{x}) = \begin{bmatrix} b_1(x) & b_2(x) & b_3(x) \end{bmatrix}^{\mathrm{T}}$, all elements can be calculated:

$$f_1(x) = 0,\ b_1(x) = 1 \tag{12}$$

$$\begin{aligned} f_2(x) &= \frac{-g(2m_1+m_2)\sin\theta_1 - gm_2\sin(\theta_1-2\theta_2) - 2m_2\left(l_1\dot{\theta}_1^2\cos(\theta_1-\theta_2) + l_2\dot{\theta}_2^2\right)\sin(\theta_1-\theta_2)}{l_1\left(2m_1+m_2-m_2\cos(2(\theta_1-\theta_2))\right)} \\ b_2(x) &= \frac{\left(-(2m_1+m_2)\cos\theta_1 + m_2\cos(\theta_1-2\theta_2)\right)}{l_1\left(2m_1+m_2-m_2\cos(2(\theta_1-\theta_2))\right)}\end{aligned} \tag{13}$$

$$\begin{aligned} f_3(x) &= \frac{2\left(l_1\dot{\theta}_1^2(m_1+m_2) + l_2m_2\dot{\theta}_2^2\cos(\theta_1-\theta_2) + (m_1+m_2)g\cos\theta_1\right)\sin(\theta_1-\theta_2)}{l_2\left(2m_1+m_2-m_2\cos(2(\theta_1-\theta_2))\right)} \\ b_3(x) &= \frac{2(m_1+m_2)\sin(\theta_1-\theta_2)\sin\theta_1}{l_2\left(2m_1+m_2-m_2\cos(2(\theta_1-\theta_2))\right)}\end{aligned} \tag{14}$$

Then the state space equations of the double pendulum can be obtained as:

$$\begin{cases} \dot{\mathbf{X}}_1 = \mathbf{X}_2 \\ \dot{\mathbf{X}}_2 = \mathbf{X}_3 \\ \dot{\mathbf{X}}_3 = \mathbf{f}(\mathbf{x}) + \mathbf{b}(\mathbf{x})u \end{cases} \tag{15}$$

The system errors are defined as:

$$\begin{aligned} \mathbf{e}_1 &= \begin{bmatrix} e_{1x} & e_{1\theta_1} & e_{1\theta_2} \end{bmatrix}^{\mathrm{T}} = \mathbf{X}_1 - \mathbf{X}_d = \begin{bmatrix} x - x_d & \theta_1 - \theta_{1d} & \theta_2 - \theta_{2d} \end{bmatrix}^{\mathrm{T}} \\ \mathbf{e}_2 &= \begin{bmatrix} e_{2x} & e_{2\theta_1} & e_{2\theta_2} \end{bmatrix}^{\mathrm{T}} = \begin{bmatrix} \dot{x} & \dot{\theta}_1 & \dot{\theta}_2 \end{bmatrix}^{\mathrm{T}} \\ \mathbf{e}_3 &= \begin{bmatrix} e_{3x} & e_{3\theta_1} & e_{3\theta_2} \end{bmatrix}^{\mathrm{T}} = \begin{bmatrix} \ddot{x} & \ddot{\theta}_1 & \ddot{\theta}_2 \end{bmatrix}^{\mathrm{T}} \end{aligned} \tag{16}$$

where $\mathbf{X}_d$ is the vector of the desired state, and $x_d, \theta_{1d}, \theta_{2d}$ are all constant.

The differential equations about system errors are defined as:

$$\begin{cases} \dot{\mathbf{e}}_1 = \mathbf{e}_2 \\ \dot{\mathbf{e}}_2 = \mathbf{e}_3 \\ \dot{\mathbf{e}}_3 = \mathbf{f}(\mathbf{x}) + \mathbf{b}(\mathbf{x})u \end{cases} \tag{17}$$

According to the Lyapunov method, the first backstepping error $\boldsymbol{\delta}_1 = \mathbf{e}_1$ is expected to converge and $\dot{V}_1(\boldsymbol{\delta}_1)$ is expected as:

$$\dot{V}_1(\boldsymbol{\delta}_1) = \boldsymbol{\delta}_1^{\mathrm{T}}\dot{\boldsymbol{\delta}}_1 = -\boldsymbol{\delta}_1^{\mathrm{T}}\mathbf{e}_2 = -\mathbf{K}_1\boldsymbol{\delta}_1^{\mathrm{T}}\boldsymbol{\delta}_1 \le 0 \tag{18}$$

so the system error $\mathbf{e}_2$ is expected to reach its virtual value $\mathbf{e}_{2d} = -\mathbf{K}_1\boldsymbol{\delta}_1$, where $\mathbf{K}_1 = diag(k_{1x}, k_{1\theta_1}, k_{1\theta_2})$ and $k_{1x}, k_{1\theta_1}, k_{1\theta_2} > 0$.

Thus, the second backstepping error is defined as $\boldsymbol{\delta}_2 = \mathbf{e}_2 - \mathbf{e}_{2d}$ and also expected to converge. $\dot{V}_2(\boldsymbol{\delta}_1, \boldsymbol{\delta}_2)$ is expected as:

$$\begin{aligned} \dot{V}_2(\boldsymbol{\delta}_1, \boldsymbol{\delta}_2) &= \boldsymbol{\delta}_1^{\mathrm{T}}\dot{\boldsymbol{\delta}}_1 + \boldsymbol{\delta}_2^{\mathrm{T}}\dot{\boldsymbol{\delta}}_2 = -\mathbf{K}_1\boldsymbol{\delta}_1^{\mathrm{T}}\boldsymbol{\delta}_1 + \boldsymbol{\delta}_2^{\mathrm{T}}(\dot{\mathbf{e}}_2 + \mathbf{K}_1\dot{\boldsymbol{\delta}}_1) \\ &= -\mathbf{K}_1\boldsymbol{\delta}_1^{\mathrm{T}}\boldsymbol{\delta}_1 + \boldsymbol{\delta}_2^{\mathrm{T}}(\mathbf{e}_3 + \mathbf{K}_1\dot{\boldsymbol{\delta}}_1) \le 0 \end{aligned} \tag{19}$$

so the system error $\mathbf{e}_3$ is expected to reach its virtual value $\mathbf{e}_{3\mathrm{d}} = \begin{bmatrix} e_{3xd} & e_{3\theta_{1d}} & e_{3\theta_{2d}} \end{bmatrix}^{\mathrm{T}} = -\mathbf{K}_1\dot{\boldsymbol{\delta}}_1 - \mathbf{K}_2\boldsymbol{\delta}_2$, where $\mathbf{K}_2 = diag(k_{2x}, k_{2\theta_1}, k_{2\theta_2})$ and $k_{2x}, k_{2\theta_1}, k_{2\theta_2} > 0$.

According to the system equation:

$$\mathbf{f}(\mathbf{x}) + \mathbf{b}(\mathbf{x})u = \mathbf{e}_{3\mathrm{d}} = -\mathbf{K}_1\dot{\boldsymbol{\delta}}_1 - \mathbf{K}_2\boldsymbol{\delta}_2 \tag{20}$$

The controller can be calculated as:

$$u = \frac{1}{\mathbf{b}(\mathbf{x})^{\mathrm{T}}\mathbf{b}(\mathbf{x})}\mathbf{b}(\mathbf{x})^{\mathrm{T}}\left[\mathbf{e}_{3\mathrm{d}} - \mathbf{f}(\mathbf{x})\right] \tag{21}$$

V. Simulation Results

The double pendulum model is simulated with the designed controller using software MATLAB/Simulink to verify its effectiveness, as shown in Fig. 6, where the system parameters are set as m_1 =3kg, m_2 =7kg, l_1 =1m, l_2 =0.5m, g =9.8m/s^2.

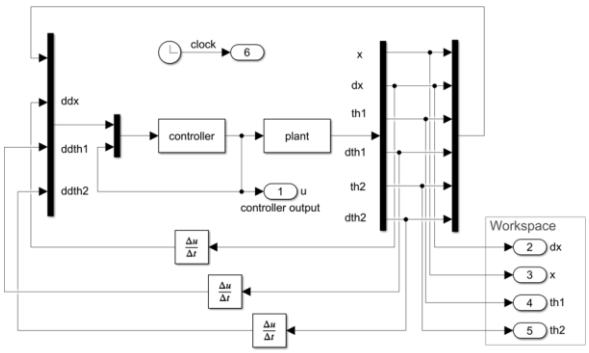

Figure 6. Simulation model of anti-swing control system based on backstepping controller

Fig. 6 shows the model of the double pendulum in Simulink. Initial states of the system are set in s-function module 'plant' as $\mathbf{x}=[x\ \ \dot{x}\ \ \theta_1\ \ \dot{\theta}_1\ \ \theta_2\ \ \dot{\theta}_2]=[0\ \ 0\ \ \pi/18\ \ 0\ \ 0\ \ 0]$, which means the first-order pendulum has a 10-degree initial angle. The parameters of the controller are set in module 'controller' as $K_1 = diag(0.92, 4, 122)$, $K_2 = diag(0.84, 2, 310)$.

All the variables in the model can be plotted during the real-time simulation run. The responses with and without the controller of the system are compared in Fig. 7. It can be seen from the response results of the system that the swing angle of the double pendulum gradually decreases and stabilizes in about 10s. The overall swing trend of both orders is similar,

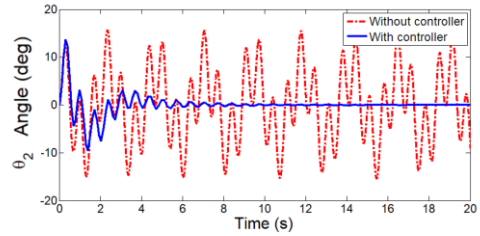

(a) Response of second-order pendulum swing angle

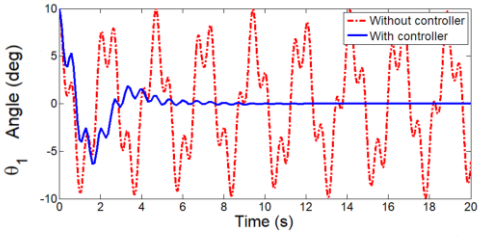

(b) Response of first-order pendulum swing angle

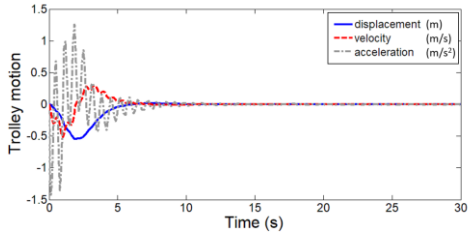

(c) Response of trolley motion

Figure 7. Response comparisons of anti-swing control system with and without backstepping controller

the residual swing of both orders almost disappears after about 15s.

Based on the above response, different main cable lengths are considered, i.e., l_1 =0.5m, 1.0m and 1.5m, respectively; l_2 =0.5m. The system response is as shown in Fig. 8. The swing of both orders of the pendulum becomes more severe as the length of the main cable increases; the amplitude of the second-order pendulum reaches about 15 degrees at its maximum. The stabilization time increases a little overall, while the displacement overshoot of the trolley decreases significantly. This means that less trolley motion is needed to balance the instabilities caused by the interference.

VI. Conclusion

In the previous chapters, the overhead crane is introduced. The dynamic modeling derivation using Lagrange equations for the double pendulum payload system of the overhead crane is described. The amplitude of the first-order pendulum and the cable length of the second-order pendulum are varied in different cases to discuss the impact on the double pendulum. Simulations for the anti-swing control system with the backstepping controller are implemented in software MATLAB/Simulink. The results show that the backstepping controller can effectively eliminate the swing induced by interference.

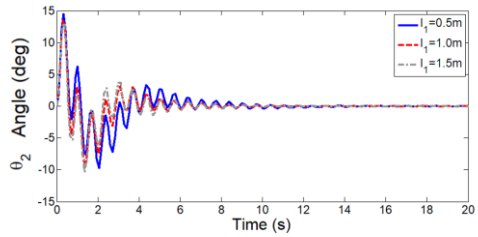

(a) Response of second-order pendulum swing angle

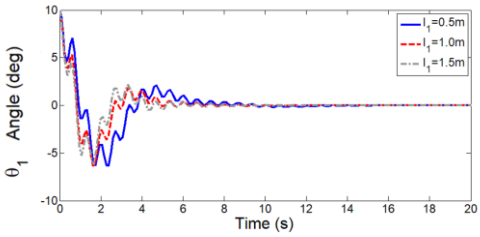

(b) Response of first-order pendulum swing angle

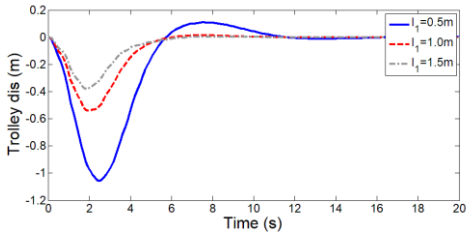

(c) Response of trolley displacement

Figure 8. Response of anti-swing control system using different cable lengths

As future works, the crane anti-swing research can also be extended to another important industrial field--offshore cranes. To derive the dynamics, Lagrange's equation can be an effective means to solve the rigid multi-body problems. However, the crane is not the product of a single discipline, but the coupling of multiple disciplines, such as hydraulics, kinematics. Further modeling approaches are yet to be discussed. In addition, the control algorithm for the double pendulum system can be more optimized according to diverse practical demands, which can also be applied to the research of offshore cranes. At this level, the real-time operation of the simulation will be considered insufficient. Field studies will be conducted based on simulation results.

REFERENCES

[1] Y. Chu, L. I. Hatledal, V. Æsøy, S. Ehlers, and H. Zhang, "An Object-Oriented Modeling Approach to Virtual Prototyping of Marine Operation Systems Based on Functional Mock-Up Interface Co-Simulation," *Journal of Offshore Mechanics and Arctic Engineering*, vol. 140, no. 2, Nov. 2017.

[2] Y. Chu, F. Sanfilippo, V. Æsøy, and H. Zhang, "An Effective Heave Compensation and Anti-sway Control Approach for Offshore Hydraulic Crane Operations," in the 2014 IEEE International Conference on Mechatronics and Automation, IEEE ICMA 2014, pp. 1282-1287, Aug. 2014.

[3] C. Liu, H. Zhao, and Y. Cui, "Research on application of fuzzy adaptive PID controller in bridge crane control system," in *2014 IEEE 5th International Conference on Software Engineering and Service Science*, pp. 971–974, Jun. 2014.

[4] S. Rishmawi, "Tip-over stability analysis of crawler cranes in heavy lifting applications," Thesis, Georgia Institute of Technology, 2016. Accessed: Jan. 17, 2022.

[5] E. M. Abdel-Rahman, A. H. Nayfeh, and Z. N. Masoud, "Dynamics and Control of Cranes: A Review," *Journal of Vibration and Control*, vol. 9, no. 7, pp. 863–908, Jul. 2003.

[6] Y. Fang, W. E. Dixon, D. M. Dawson, and E. Zergeroglu, "Nonlinear coupling control laws for an underactuated overhead crane system," *IEEE/ASME Trans. Mechatron.*, vol. 8, no. 3, pp. 418–423, Sep. 2003.

[7] D. Qian, S. Tong, and S. Lee, "Fuzzy-Logic-based control of payloads subjected to double-pendulum motion in overhead cranes," *Automation in Construction*, vol. 65, pp. 133–143, May 2016.

[8] H. M. Omar and A. H. Nayfeh, "Anti-Swing Control of Gantry and Tower Cranes Using Fuzzy and Time-Delayed Feedback with Friction Compensation," *Shock and Vibration*, vol. 12, no. 2, pp. 73–89, 2005.

[9] K. Nakazono, K. Ohnishi, H. Kinjo, and T. Yamamoto, "Vibration control of load for rotary crane system using neural network with GA-based training," *Artif Life Robotics*, vol. 13, no. 1, pp. 98–101, Dec. 2008.

[10] S. C. Duong, E. Uezato, H. Kinjo, and T. Yamamoto, "A hybrid evolutionary algorithm for recurrent neural network control of a three-dimensional tower crane," *Automation in Construction*, vol. 23, pp. 55–63, May 2012.

[11] M. I. Solihin, Wahyudi, and A. Legowo, "Fuzzy-tuned PID Anti-swing Control of Automatic Gantry Crane," *Journal of Vibration and Control*, vol. 16, no. 1, pp. 127–145, Jan. 2010.

[12] N. B. Almutairi and M. Zribi, "Fuzzy Controllers for a Gantry Crane System with Experimental Verifications," *Mathematical Problems in Engineering*, vol. 2016, pp. 1–17, 2016.

[13] N. B. Almutairi and M. Zribi, "Sliding Mode Control of a Three-dimensional Overhead Crane," *Journal of Vibration and Control*, vol. 15, no. 11, pp. 1679–1730, Nov. 2009.

[14] Z. Wu, X. Xia, and B. Zhu, "Model predictive control for improving operational efficiency of overhead cranes," *Nonlinear Dyn.*, vol. 79, no. 4, pp. 2639–2657, Mar. 2015.

[15] N. Sun, Y. Fang, H. Chen, and B. Lu, "Amplitude-Saturated Nonlinear Output Feedback Antiswing Control for Underactuated Cranes With Double-Pendulum Cargo Dynamics," *IEEE Trans. Ind. Electron.*, vol. 64, no. 3, pp. 2135–2146, Mar. 2017.

[16] M. W. Spong, S. Hutchinson, and M. Vidyasagar, *Robot modelling and control*. John Wiley & Sons, 2005.

[17] D. Liu, J. Yi, D. Zhao, and W. Wang, "Adaptive sliding mode fuzzy control for a two-dimensional overhead crane," *Mechatronics*, vol. 15, no. 5, pp. 505–522, Jun. 2005.